How to assess the layers' thicknesses in polymer-coated cardboards?

Allison Vercasson, Sébastien Gaucel, Sébastien Destercke, Nathalie Gontard, Valérie Guillard, Helene Angellier-Coussy

▶ **To cite this version:**

Allison Vercasson, Sébastien Gaucel, Sébastien Destercke, Nathalie Gontard, Valérie Guillard, et al.. How to assess the layers' thicknesses in polymer-coated cardboards?. Progress in Organic Coatings, 2024, 193, pp.108532. 10.1016/j.porgcoat.2024.108532 . hal-04614643

HAL Id: hal-04614643
https://hal.inrae.fr/hal-04614643

Submitted on 17 Jun 2024

HAL is a multi-disciplinary open access archive for the deposit and dissemination of scientific research documents, whether they are published or not. The documents may come from teaching and research institutions in France or abroad, or from public or private research centers.

L'archive ouverte pluridisciplinaire **HAL**, est destinée au dépôt et à la diffusion de documents scientifiques de niveau recherche, publiés ou non, émanant des établissements d'enseignement et de recherche français ou étrangers, des laboratoires publics ou privés.

Distributed under a Creative Commons Attribution - NonCommercial - NoDerivatives 4.0 International License

Progress in Organic Coatings 193 (2024) 108532

Contents lists available at ScienceDirect

Progress in Organic Coatings

journal homepage: www.elsevier.com/locate/porgcoat

How to assess the layers' thicknesses in polymer-coated cardboards?

Allison Vercasson [a], Sébastien Gaucel [a], Sébastien Destercke [b], Nathalie Gontard [a], Valérie Guillard [a], Hélène Angellier-Coussy [a,*]

[a] JRU IATE, University of Montpellier, INRAE, Institut Agro, 2 Place Pierre Viala, 34060 Montpellier, France
[b] Compiègne University of Technology, CNRS, Heudiasyc, CS 60 319, 60 203 Compiègne Cedex, France

ARTICLE INFO

Keywords:
Multilayered structure
Coated cardboard
Impregnation
Thickness determination
Image analysis
Sample preparation

ABSTRACT

When polymers are coated on the surface of cardboards, they inevitably penetrate through the cardboard pores, resulting in a complex three-layer structure consisting of a free polymer layer, an impregnated layer, and a free cardboard layer. In this article, two quantitative, representative, and reliable methods are proposed to determine the thickness of the individual layers, which is an indispensable prerequisite for deciphering the role of multi-layer structures on the final properties of polymer-coated cardboards. The first method involves the analysis of images obtained either by scanning electron microscopy (SEM) or X-ray microtomography. The second method proposes a modeling approach based on experimental measurements of macroscopic physical parameters. The two methods provide congruent information but differ in terms of accessibility and precision. The main challenge with the SEM-based method lies in the cutting technique required to obtain clean cross-sections. X-ray micro-tomography does not require sample preparation, but its accuracy is lower. The main issue of the modeling approach is the quantitative and representative evaluation of the cardboard's porosity. Finally, both methods provided consistent results, e.g. with impregnated layers thicknesses of [257–270] and [167–247] µm for PHBV- and LLDPE-coated cardboards, respectively, highlighting a total and a partial impregnation. These methods can be used to detect not only an impregnated layer, but also an impregnation gradient in the coated cardboard, which needs to be further studied.

Nomenclature

List of abbreviations

C1	Uncoated Cup Forma
C2	Uncoated blotting paper
LLDPE	Low linear density polyethylene
PHBV	Poly(3-hydroxybutyrate-*co*-3-hydroxyvalerate)
$d_{cellulose}$	Cellulose density (g·cm^{-3})
$d_{polymer}$	Polymer's density (g·cm^{-3})
m_c	Control cardboard's mass (g)
m_{cc}	Coated cardboard's mass (g)
m_{uc}	Uncoated cardboard's mass (g)
S_c	Control cardboard's surface (m^2)
S_{cc}	Coated cardboard's surface (m^2)
S_{uc}	Uncoated cardboard's surface (m^2)
bw_c	Control cardboard's basis weight (g·m^{-2})
bw_{cc}	Coated cardboard's basis weight (g·m^{-2})
bw_{uc}	Uncoated cardboard's basis weight (g·m^{-2})
cw	Polymer's coating weight (g·m^{-2})
V_c	Control cardboard's volume (m^3)
V_i	Impregnated layer's volume (m^3)
$V_{p,i}$	Volume of polymer that has impregnated the cardboard (m^3)
V_{pores}	Cardboard pores' volume (m^3)
ϕ_a	Porosity accessible to the polymer
ϕ_c	Control cardboard's porosity
k	Porosity coefficient
l_c	Control cardboard's thickness (µm)
l_{cc}	Coated cardboard's thickness (µm)
l_p	Theoretical polymer thickness (µm)
l_{fp}	Free polymer layer thickness (µm)
l_i	Impregnated layer thickness (µm)
l_{fc}	Free cardboard layer thickness (µm)

1. Introduction

Paper and cardboard could be an excellent alternative to

* Corresponding author.
E-mail addresses: allison.vercasson@umontpellier.fr (A. Vercasson), sebastien.gaucel@inrae.fr (S. Gaucel), sebastien.destercke@hds.utc.fr (S. Destercke), nathalie.gontard@inrae.fr (N. Gontard), valerie.guillard@umontpellier.fr (V. Guillard), helene.coussy@umontpellier.fr (H. Angellier-Coussy).

https://doi.org/10.1016/j.porgcoat.2024.108532
Received 12 March 2024; Received in revised form 10 May 2024; Accepted 17 May 2024
Available online 25 May 2024
0300-9440/© 2024 The Authors. Published by Elsevier B.V. This is an open access article under the CC BY-NC-ND license (http://creativecommons.org/licenses/by-nc-nd/4.0/).

conventional fossil-based and persistent plastics, provided that their very low barrier properties and high hydrophobicity are overcome while maintaining their recyclability and complete biodegradability. Coating paper or cardboard with thin films of biobased, biodegradable biopolymer with high barrier properties and water resistance seems to be the most promising alternative, as already reported by several authors [1–4].

When applying a polymer coating to a porous and fibrous cellulose, such as cardboard, part of the coated polymer inevitably penetrates the cellulose substrate, as reported in several papers [4–11]. This polymer impregnation leads to the formation of a complex multilayered structure with at least three layers, i.e., a dense polymer coating layer (corresponding to the polymer that does not impregnate the cellulose substrate), an impregnated layer, and a non-impregnated cellulose substrate [5–7,11]. The macroscopic properties of multilayer materials depend on the intrinsic properties and structure of the individual compartments, as well as on the properties of the interfaces [12]. It is therefore assumed that the presence of an impregnated layer, which would exhibit properties that differ significantly from those of the bulk polymer or cellulose substrate, may influence the coated cardboards properties. Knowledge of the structure of such multilayer systems, and at least quantitative characterization of the thickness of each layer, is necessary to control and predict the functional properties, which remains a key challenge for polymer-coated cardboards or papers.

The presence of an impregnated layer has rarely been studied or even noticed. Often, the main research topic does not need to consider the presence of coating impregnation into the cardboard or paper, as this is not the aim of the research [13–16]. However, when observations, SEM, or calculations highlight some differences in the results, such as a decrease in coating thickness, the impregnation process may be mentioned but its effects have not been further investigated [10,17,18]. For example, Samyn et al. [10] and Sundar et al. [17] both mentioned the impregnation of the coating into the cardboard when they observed a decrease in coating thickness while Türe et al. [18] observed a difference in tensile property values that could be explained by the impregnation process, but they all did not investigate this phenomenon further. When the presence of an impregnated layer is investigated, it is usually characterized qualitatively by scanning electron microscopy (SEM) [3,5–7,9], optical microscopy [19,20] observations, and/or X-ray tomography [21–24]. In some studies, microscopic observations were coupled with image analysis to thoroughly investigate the 2D structure, for example with confocal laser scanning microscopy (CLSM), focused ion beam scanning electron microscopy (FIB-SEM) [25–27] or backscattered electron microscopy (BSE-SEM) [7,16]. X-ray computed tomography can also be used in conjunction with 3D reconstruction algorithms [24], as has been done to characterize papers [28–30] and to understand liquid penetration [25]. Several papers investigating porous structures, not only focused on papers and cardboards, and are able to obtain information regarding pore systems such as porosity, pore interconnectivity of 3D-pore network by using computational techniques [8,31–41]. It is worth noting that such imaging techniques sometimes require a modification of the polymer by adding a fluorescent dye to facilitate visualization of the polymer distribution in the cellulose substrate [7,8,11], which can lead to a change in the structure of the material as the fibers swell. In addition, most microscopy techniques require a clean cut of the material cross-section without mixing the layers or damaging the fibers to allow good visualization of the different layers, which is a difficult step for porous substrates. Special cutting techniques such as cryofracture [6,17,42,43], microtome [20,22,26], cryo-ultramicrotome [44] or resin embedment [7,16,45] have already been used successfully, but the latter are either expensive, lead to the swelling of the cellulose fibers and/or do not allow precise determination of the layer thicknesses [3]. In summary, although the characteristic layers of polymer-coated cardboards can be visualized using imaging techniques, none of these studies went so far as to quantify the thicknesses of the individual layers, which makes them useless for further modeling approaches.

Some authors have attempted to estimate an impregnation percentage, i.e. the difference between the expected and apparent coating thicknesses divided by the expected coating thickness, based on the calculation of the apparent polymer coating thickness [20,46], but have not reported the actual values of the thicknesses. The most advanced studies are those of Khlewee et al., which deal with the investigation of the impregnation mechanisms of an adhesive in paper [47,48]. They succeeded in determining the thickness of the impregnated layer using an easy-to-implement technique based on oil absorption in the materials. However, the thicknesses of the free adhesive layer and the free paper layer, which are necessary for further prediction of the overall properties of the multilayer, were not mentioned.

In this context, the aim of this paper is to investigate and compare two quantitative, representative, and reliable methods for determining the thickness of the individual layers in polymer-coated cardboards, including the impregnated layer. For this purpose, four polymer-coated cardboards with different degrees of impregnation were produced by selecting two types of carboards (a commercial cardboard as a commercial reference substrate and an untreated blotting paper to emphasize the polymer impregnation phenomenon) and two polymers: poly(3-hydroxybutyrate-*co*-3-hydroxyvalerate) (PHBV), a biopolymer having a low melt viscosity and a high melting point, and linear low-density polyethylene (LLDPE), a conventional polymer with a higher melt viscosity and a lower melting point, as reference for coating polymers. The first method is based on image acquisition (either by scanning electron microscopy or X-ray microtomography) and analysis. The second method relies on the use of an analytical model based on experimental measurements of macroscopic physical parameters (including mass, surface area, total thickness, density and porosity). The novelty of this research is that, for the first time, a complete estimation of the thickness of each layer in a multilayer cardboard-based system is proposed.

2. Materials and methods

2.1. Materials

A commercial cardboard (Cup Forma Natura, Stora Enso, Stockholm, Sweden, basis weight of 260 ± 1 g.m^{-2} and thickness of 370 ± 2 µm, noted C1) and an untreated blotting paper (Centre Technique du Papier, Grenoble, France, basis weight of 248 ± 3 g.m^{-2} and thickness of 460 ± 4 µm, noted C2) were used as cellulose substrates. Cardboards and untreated blotting papers used as received (i.e., without further coating or processing) are referred to as “uncoated cardboards”. Both materials were stored for at least 24 h at 50 % relative humidity and 23 °C before use.

Two commercially available polymers, with different properties (Table 1), were used as polymer coatings to enable the production of coated cardboards with different structures. Poly(3-hydroxybutyrate-*co*-3-hydroxyvalerate) (PHBV), density of 1.24 g.cm-3, was purchased from Natureplast (Mondeville, France) in the form of a powder under the reference PHI003. Linear low-density polyethylene (LLDPE), density of 0.92 g.cm^{-3}, was supplied by ExxonMobil Chemical (LL 1002YB, Irvin, USA) in the form of pellets. Both polymers were dried at 60 °C for 24 h before use.

Table 1
Properties of LLDPE and PHBV.

Polymer	Melting temperature (°C)	Degradation temperature (°C)	Melt flow index (g/10 min - 190 °C – 2.16 kg)
PHBV	172	242	15–30[a]
LLDPE	123	390	2[a]

[a] Obtained from supplier.

2.2. Preparation of coated papers

Around 10 × 10 cm square self-supported polymer films with a thickness of 100 µm were prepared by thermocompression using a hydraulic heating press (LAB 800 PA, Pinette Emidecau Industries, Chalon-sur-Saône, France) in two steps. First, the polymer was placed between two Teflon sheets and brought into contact with the heating plates for 10 min at the desired temperature to ensure sufficient melting of the polymer at temperatures of 180 °C for PHBV and 140 °C for LLDPE. Then, successive pressures of 50, 100 and 150 bars were applied, for 30, 30 and 60 s respectively. The resulting polymer films were then placed on approximately 10 × 10 cm cellulose substrates between the two Teflon films for another thermocompression cycle. The same thermocompression procedure was used, but the duration of the first contact was shortened to 5 min.

Control cardboards were produced by applying a thermocompression procedure to an approximately 10 × 10 cm square of uncoated cardboard, to obtain a structure close to the cellulose substrate present in coated cardboards. The thermocompression process was the same as that used to coat the polymer on the cardboard.

The produced coated cardboards were stabilized at 23 °C and 50 % relative humidity for 14 days to allow the secondary crystallization of PHBV [49]. They were then stored in hermetic boxes and protected from direct light before being further characterized. The resulting polymer-coated cardboards were coded as "Ci_j", $i = \{1,2\}$, $j = \{PHBV, LLDPE\}$, where C1 and C2 refer to the Cup Forma and the untreated blotting cardboard, respectively, e.g., C1_PHBV stands for the Cup Forma cardboard coated with PHBV.

The structure of the polymer-coated cardboards can be represented in two ways. In the theoretical case where no polymer is impregnated into the cardboard, the structure of the coated cardboard is represented as a two-layer structure composed of a polymer coating layer of thickness l_p and a cardboard layer of thickness l_c (Fig. 1a). In contrast, in the case of polymer impregnation, the material can be represented by a three-layer structure consisting of a free polymer layer of thickness l_{fp}, an impregnated layer of thickness l_i, and a non-impregnated free cardboard layer of thickness l_{fc} (Fig. 1b). It is assumed that the overall cardboard thickness is constant, $l_c = l_i + l_{fc}$, as no significant swelling of the cardboard was observed in the present study.

2.3. Materials characterization

2.3.1. Thickness

The thickness of the material was measured using a digimatic micrometer (0–25 mm, MDC-25SX, Mitutoyo Co. Ltd., Tokyo, Japan) with an accuracy of 0.001 mm, with taking 10 different measuring points evenly distributed on the surface of the material (Fig. S1).

2.3.2. Mass

The samples of control cardboard (c), uncoated cardboard (uc), and coated cardboard (cc) were weighed using a 4-digit balance (LX 220 A, BALCO, Switzerland) and the corresponding masses (in g) were noted as m_c, m_{uc}, and m_{cc}, respectively. The measurements were carried out in duplicate.

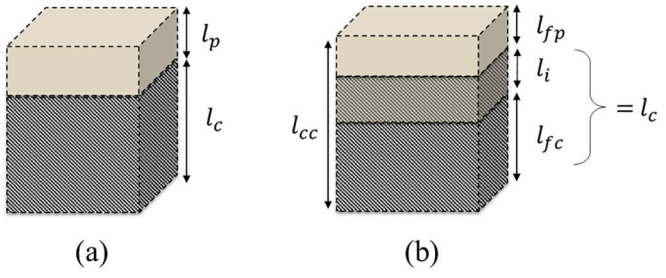

Fig. 1. (a) Bilayer structure without impregnation and (b) three-layer structure with impregnation of polymer-coated cardboards.

2.3.3. Surface area

The materials were scanned using a scanner (MP3555, 600 dpi, RICOH, Tokyo, Japan). Their surface areas (in m^2), noted as S_c, S_{uc}, and S_{cc} for the surface areas of control cardboard, uncoated cardboard, and coated cardboard, respectively, were determined using image analysis (Fiji software, v.1.54f) [50].

2.3.4. Basis weight

The different basis weights (in $g.m^{-2}$) were calculated using Eq. (1):

$$bw_i = \frac{m_i}{S_i} \quad (1)$$

where $i = \{c; uc; cc\}$ for the control cardboard, the uncoated cardboard, and the coated cardboard, respectively.

For each polymer-coated carboard, the coating weight (noted *cw*, in $g.m^{-2}$) was calculated according to Eq. (2):

$$cw = bw_{cc} - bw_{uc} \quad (2)$$

2.3.5. Cardboard porosity

2.3.5.1. Estimated average porosity. The porosity of cardboard (noted ϕ) was calculated according to Eq. (3), where l is the paper thickness (in µm), *bw* the paper basis weight (in $g.m^{-2}$) and $d_{cellulose}$ the cellulose density (considered equal to 1.5 $g.cm^{-3}$) [51]. This porosity value corresponds to the average porosity of the paper, without distinguishing between surface and bulk porosity.

$$\phi = 1 - \frac{bw}{l \times d_{cellulose}} \quad (3)$$

2.3.5.2. Mercury porosimetry. Mercury porosimetry was carried out using a Poremaster 60 (Quantachrome, Anton Paar, Graz, Austria). The surface tension (γ) and the contact angle (θ) were considered with 480 mN/m and 140°, respectively. The pore diameter is calculated using the Washburn's equation (Eq. (4)):

$$D = -4 \times \frac{\gamma \times cos(\theta)}{P} \quad (4)$$

with D the pore diameter (nm), and P the applied pressure (MPa).

2.3.6. Scanning electron microscopy (SEM)

Different cutting techniques were tested to prepare the samples for SEM image acquisition. An ultramicrotome (LEICA UC6, LEICA, Wetzlar, Germany), equipped with a cryo-chamber, was used at −130 °C and an angle of 35° (cryo-ultramicrotome). A manual microtome (WSL-Lab-Microtome, Schenkung Dapples, Zürich, Switzerland) was used with two types of blades, a razor and a cutter blade, and samples were cut at an angle of 45°. A cut of the sample included in a wood pith has been performed using a razor-blade aligned perpendicular to the sample. For ultramicrotome cuts, a ultramicrotome (LEICA UC7, LEICA, Wetzlar, Germany) was used. Samples cut using scissors, a razor blade, or a cutter blade, where cut perpendicular to the sample. The last cut was performed immerging the sample in liquid nitrogen for a few seconds before folding it to induce the cut.

The cross-sections of the coated and uncoated cardboards were observed using a scanning electron microscope with an acceleration voltage of 2.5 kV. Depending on the cutting technique, three different microscopes were used. Indeed, to prevent the sample from being damage, which may occur during transportation, which would lead to a deterioration of the sample's cross-section, the samples were analyzed using the closest SEM to the location where the cutting technique was performed. For cross-sections obtained using a cryo-ultramicrotome, a

FEI QUANTA-FEG 250 was used (Thermo Fisher Scientific Inc., Massachusetts, USA). When using the ultramicrotome, a FEI QUANTA-FEG 200 was used (Thermo Fisher Scientific Inc., Massachusetts, USA). Samples obtained using other cutting techniques were observed using a Phenom ProX (Thermo Fisher Scientific Inc., Massachusetts, USA). Prior to analysis, all materials were metallized with gold/palladium using an ion sputter coater.

For the SEM observations of the samples cut using the cryo-ultramicrotome techniques, 3 observations were made for both PHBV and LLDPE C2-coated cardboards, and 1 for each C1-coated cardboard.

2.3.7. X-ray microtomography (μCT)

A microtomograph (EasyTom 150, RX Solutions, Chavanod, France) was used to characterize the material structure. The voxel size was 5 × 5 μm. The three-dimensional data sets were cut from two-dimensional cross-sectional images of the materials to determine the different characteristic thicknesses (total, free polymer, impregnation, free cardboard).

2.3.8. Image analysis

The SEM and microtomography images were first straightened and cropped in the same dimensions using Fiji software [50]. The resulting images were analyzed using a developed MATLAB code (The MathWorks Inc., Natick, Massachusetts, USA), under Windows 11 (v.23H2, Microsoft, Redmond, USA).

3. Results and discussion

3.1. Assessment of thicknesses using image acquisition and analysis

A first approach to directly determine the thickness of the different layers of polymer-coated cardboards is the quantitative analysis of cross-sectional images obtained from microscopic observations. In the case of SEM observations, a clean cut of the materials is required, which represents the biggest challenge as it directly affects the visualization and the resulting observations and conclusions, is necessary.

3.1.1. Qualitative observations of cross-sections by SEM and X-ray microtomography

The C1_LLDPE was used as a reference to compare the different cutting techniques tested to obtain the cleanest cut for the best visualization of the actual structure of the coated cardboard and to allow the characterization of the layer's thicknesses.

A total of nine techniques were investigated: (A) cryo-ultramicrotome, (B) manual microtome with a cutter blade, (C) inclusion in wood pith and razor blade, (D) ultramicrotome, (E) scissors, (F) razor blade, (G) manual microtome with a razor blade, (H) cutter blade, and (I) cryofracture.

First, except for cryofracture, the presence of a free polymer layer could be qualitatively demonstrated with all tested techniques (Fig. 2). Both the evaluation of other layers and the characterization of thicknesses were not possible most techniques. It has been shown that the use of a cutter blade or cryofracture led to a destruction of the overall

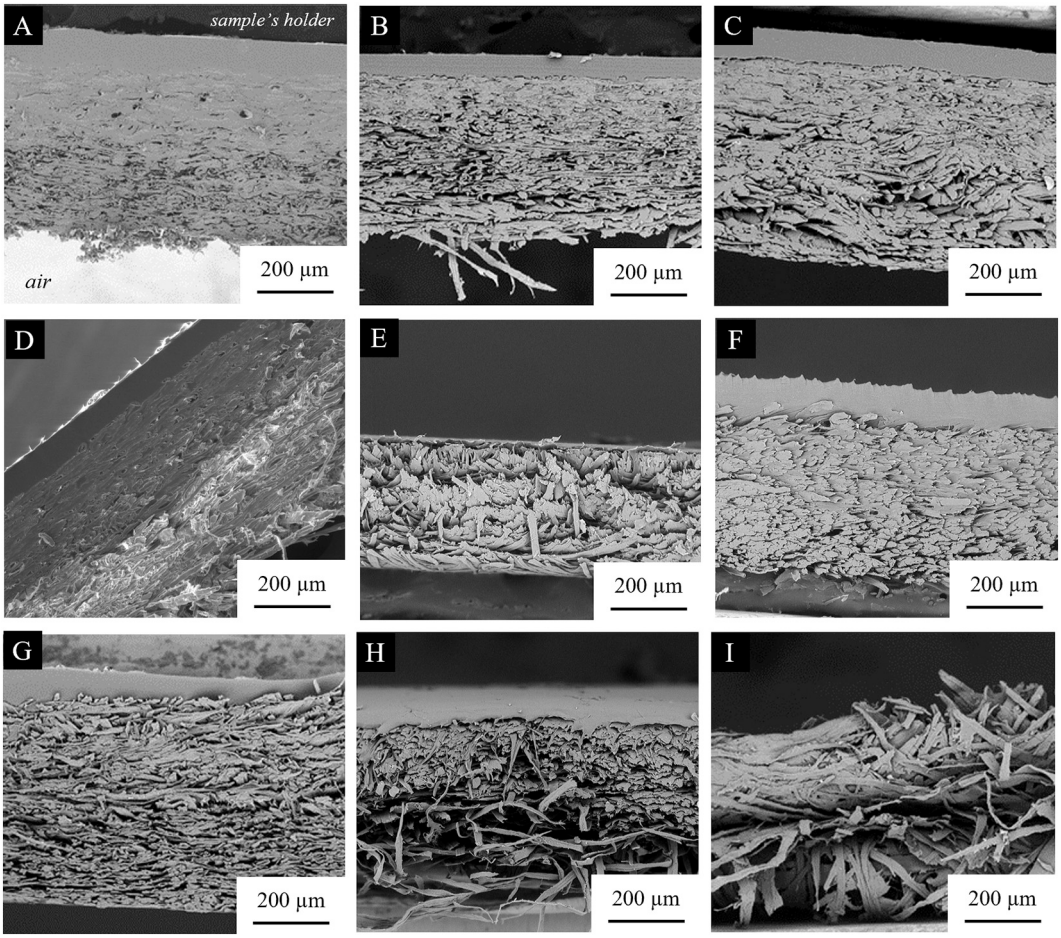

Fig. 2. SEM observations of LLDPE-coated cardboard's cross-sections (C1_LLDPE) using different cutting techniques: (A) cryo-ultramicrotome, (B) manual microtome with a cutter blade, (C) inclusion into wood pith and razor blade, (D) ultramicrotome, (E) scissors, (F) razor blade, (G) manual microtome with a razor blade, (H) cutter blade, and (I) cryofracture. The polymer layer is facing upwards in the images.

structure (Fig. 2H and I), thus preventing the visualization of all layers. Cryofracture is a very common technique that has been used successfully in the literature for coated papers and cardboards. Sundar N. et al. [17] have obtained cross-sectional images that serve as supporting data for the contact angle and surface roughness analyses. These cross-sections allow the detection of a free polymer layer. However, it should be noted that the coated papers considered in their study were thinner than those presented in this article (150 μm vs. 350 μm approximately), which could explain the difference in results [17]. Adibi A. et al. [43] also used cryofracture, but on a thicker coated cardboard, to check the homogeneity of the coating layer on the paper surface and its ability to fill the surface porosity. The authors obtained cross-sections that made possible to visualize the free polymer layer, but it was still not possible to distinguish the other layers [43].

The use of scissors, a razor blade or a manual microtome with a razor blade allowed to observe the free polymer layer on the top of the material, but led to a change, a tearing, of the cardboard structure (Fig. 2E, F and G). The tearing of the cardboard layer hampered the accurate measurement of both the cardboard layer and the free polymer layer. Even though techniques such as scissors, razor blades and cutter blades are readily available, they are not an efficient solution for determining the coated cardboard's thickness (Fig. 2E, F and H), confirming previous conclusions made by various authors. In the literature, Han J. & Krochta J. used blades to obtain cross-sections of coated cardboards and were unable to detect the free coating layer due to the fuzziness of the cross-section, except for the coated cardboard with the highest coating weight [52]. However, the authors were able to demonstrate the fulfillment of surface porosity by the coating and the decrease in roughness. On the other hand, Khlewee M. et al. were unable to obtain a clean cross-section of coated cardboards using a razor blade but were still able to evidence the impregnation of the glue in the cardboard [47].

The four remaining techniques, i.e., cryo-ultramicrotome, manual microtome combined with a cutter blade, inclusion into a wood pith and ultramicrotome, showed a clear view of the free polymer layer, which allowed evaluation of the thickness of the free polymer layer (Fig. 2A, B, C and D). However, cuts obtained using the manual microtome combined with a cutter blade or the inclusion into a wood pith compromised the structure of the cardboard, i.e., they presented a blurring of the cardboard, tearing of the fibers and partial detachment of the polymer layer. Consequently, it was not possible to investigate the presence of an impregnated layer with these techniques, which made it difficult to measure the thickness of the cardboard layer's thickness. Aslannejad J. et al. [26] were able to obtain a clear cross-section of coated cardboards using a manual microtome to examine the interface between the coating and the base paper, where both the free polymer and the impregnated layer were visible. However, they were not able to observe the entire thickness of the free cardboard layer [26].

Finally, using the cryo-ultramicrotome and the ultramicrotome, three different layers could be observed (Fig. 2A, D). Theoretically, both techniques could have been used to evaluate the layer thicknesses. However, the samples obtained with the ultramicrotome showed a slight change in the cardboard structure (i.e. the fibers were flattened), which resulted in a lower precision of the images. Gastaldi E. et al. [20] successfully used the ultramicrotome to obtain a clean cross-section, but on samples that had previously been immersed in resin. They showed that staining of the polymer prior to sectioning was necessary to identify the impregnated layer [20].

It is worth noting that techniques altering the sample such as serial sectioning, which requires resin embedment of the sample, were not considered in this study as they may induce structural changes in the sample. The objective was to observe the actual cross-section and layer thicknesses, without further modification. Indeed, the coated carboard inclusion in resin could lead to an impregnation of the resin within the cellulosic substrate, thus hindering the distinction between polymer impregnation and resin impregnation or modifying the arrangement of the fibers. This would make it more difficult to determine the actual impregnated thickness.

Also, when using different cutting techniques, different metallizer were used on samples which led to difference in contrast on the resulting SEM images, but do not impact the visualization of layers.

To conclude, although some easily accessible techniques such as scissors or razor blades can be used to evidence the free polymer layer, the use of a cryo-ultramicrotome, i.e. an ultramicrotome under cryogenic conditions, seems to be a prerequisite to obtain a clear visualization of all three layers of the coated cardboards and to further evaluate their thickness. This technique was therefore further used to prepare additional samples for image acquisition and analysis.

Cross-sections of different materials cut with the cryo-ultramicrotome were visualized by SEM (Fig. 3). Depending on the type of polymer coating, i.e. PHBV or LLDPE, different structures were obtained. For LLDPE-coated cardboards, three different layers were observed, corresponding respectively, from top to bottom, to the free polymer layer, the impregnated layer, and the free cardboard layer (Fig. 3C and F). The free LLDPE layer appears to be homogeneous. The presence of a free polymer coating layer has already been confirmed, as it has already been observed in the literature [6,10,19,53]. For PHBV-coated cardboards, only a heterogeneous layer was visible (Fig. 3B and E), while both the free polymer and free cardboard layers do not appear to be present. This indicates that the PHBV has completely impregnated the cardboard. These different degrees of impregnation could be explained by the difference in melt viscosity of the two polymers. PHBV has a higher melt flow index than LLDPE, namely 51.6 and 5.4 g/10 min for PHBV [54] and LLDPE [55], respectively, therefore emphasizing the PHBV penetration into the cardboard's open pores. Also, LLDPE presents a faster crystallization rate than PHBV (no addition of nucleating agent in the present study), which might allow the PHBV to pursue its impregnation into the cardboard after the thermocompression until its full crystallization. It is worth noting that both for C1 and C2 coated cardboards, a residual porosity seems to be visible in the impregnated layer. This can be due to the presence of either closed pores or pores that cannot be reached by the polymer. Literature defined cardboards pores as macropores (i.e., above 0.1 μm) [48] and as open pores [56]. The porosity of the control cardboards was determined using mercury porosimetry and resulted in a porosity of 53 ± 1 %, which was in the same order of magnitude as the porosity calculated from Eq. (3) (48 %) (Fig. S2). However, this open porosity might not be fully accessible to the polymer, due to the higher gyration radius of the polymer compared to mercury. Part of the total pore volume is not available for impregnation, so the polymer front must penetrate deeper in the cardboard. Such observations regarding the presence of empty pores in the impregnated layer can also be derived from the literature [5,53].

Another explanation could be that apparently closed pores are due to the tearing of some fibers during cutting, leading to holes in the impregnated layer. However, X-ray tomography images that did not require cutting also showed similar pores (Fig. 4), confirming the actual presence of these pores.

2D-images of the cross-sections of both C1-coated cardboards were also obtained by X-ray microtomography analysis. For C1_PHBV, there was no evidence of a free polymer layer on the top of the material nor of a free cardboard layer on the bottom (Fig. 4B). It appears that the polymer has impregnated the cardboard completely, but not homogeneously, as indicated by the presence of fewer pores in the upper half of the material. This could be due to the presence of an impregnation gradient in the coated cardboard, where the concentration of the polymer decreases from the top to the bottom of the sample. While a partial impregnation of the polymer coating has already been demonstrated in the literature, either with wheat gluten [5] or a pigment binder [7], to the best of our knowledge, no complete impregnation of PHBV in a cellulose substrate has yet been observed. For C1_LLDPE, the three different layers could be clearly distinguished, especially the free polymer layer (Fig. 4A).

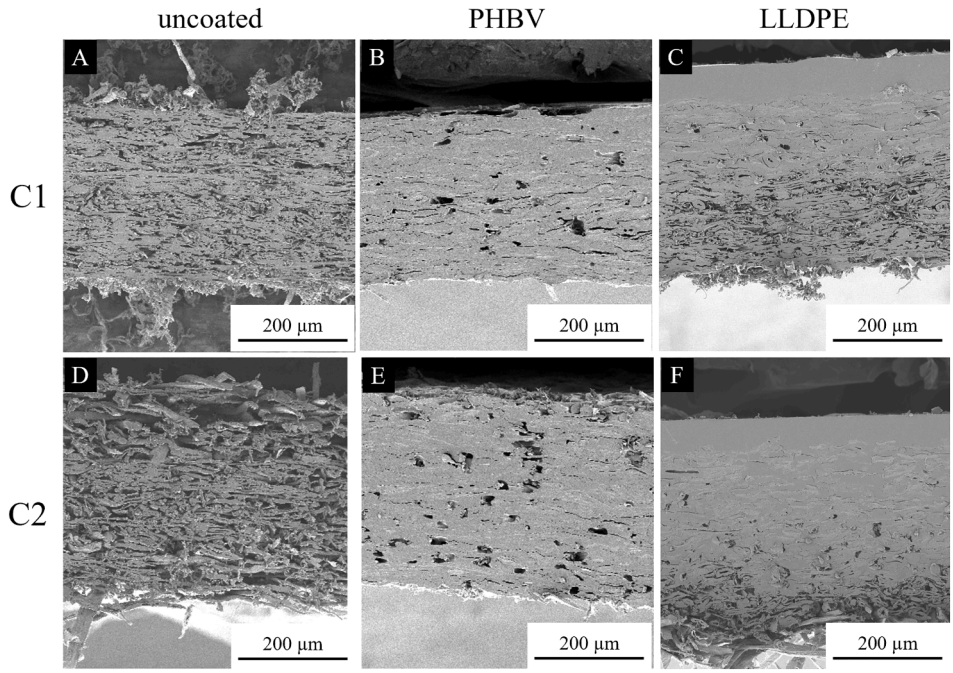

Fig. 3. SEM images of cross-sections of both control and polymer-coated cardboards obtained using a cryo-ultramicrotome: (A) control C1, (B) C1_PHBV, (C) C1_LLDPE, (D) control C2, (E) C2_PHBV, (F) C2_LLDPE (see dataset, doi:10.57745/D63VYY).

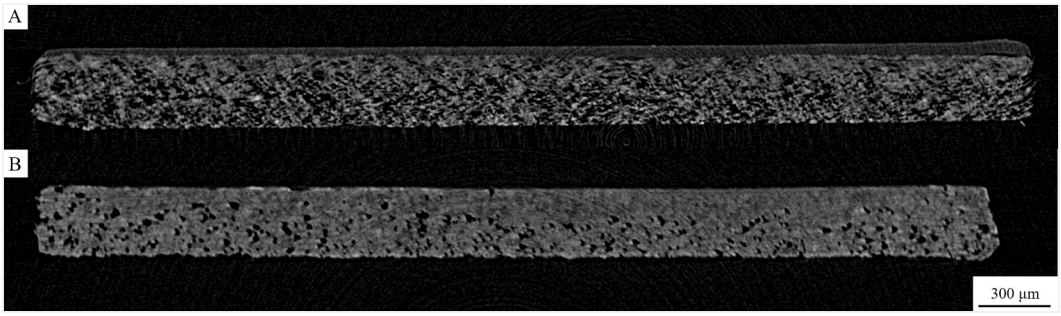

Fig. 4. Cross-sections of (A) C1_LLDPE and (B) C1_PHBV obtained by microtomography (see dataset, doi:10.57745/D63VYY).

3.1.2. Quantitative assessment of thicknesses through image analysis

To quantitatively evaluate the thickness of each layer by image analysis, a method was developed based on that used by Le Duigou et al. [57] and Shirazi et al. [11]. It consists of determining, for each image obtained, the grey intensity profile for a column of pixels, i.e. along the thickness of the materials. The mean profile of all vertical pixel's rows and the corresponding variance are plotted as a function of the material thickness. The plots obtained for C1- and C2-coated cardboards are shown in Fig. 5. The analysis of the replicates for C2-coated cardboards, exhibiting the same behavior, and for uncoated C1 and C2 can be found in Supplementary materials (Fig. S3). In Fig. 5, each plot is linked to the corresponding SEM image.

For C1_LLDPE, the boundaries between the coated cardboard, and the environment, i.e. the atmosphere or the mount, can be evidenced by two peaks of pixel intensity variance, allowing to assess the thickness of the coated cardboard (Fig. 5). However, it should be noted that the intensity and the position of these peaks strongly depends on the quality of the sample's preparation. Indeed, tearing of the cellulose fibers on the cardboard side was observed in some samples, while artefacts appeared at the sample-mount interface, possible leading to a scattering, or shifting of the variance peaks (see Fig. S4). When determining the thicknesses, the values at the tip of the peak under consideration are considered.

From left (coated cardboard – mount boundary) to right (coated cardboard – outer atmosphere), the free polymer layer was characterized by a first curve section, with a constant mean intensity and a constant and very low variance, both related to the homogeneity of the polymer layer. It corresponds to the range [43;107] µm and [38;97] µm for samples C1_LLDPE and C2_LLDPE respectively. Although the presence of the free polymer layer was qualitatively indisputable, interferences were observed in some samples that required an adjustment of the thickness determination. Indeed, some pieces of fibers or dust were observed on the surface of the section, located on the free polymer layer (Fig. S3, C2_LLDPE (4)). It is suspected that these elements were created during cutting and then redeposited on the sample surface before metallization and imaging. They must therefore be removed from the image analysis if the thicknesses are to be determined. The value of the thickness of the free polymer layer was determined by considering the maximum of the first peak related to the beginning of the coated cardboard, and the next first peak after stabilization of the variance corresponding to the free polymer layer.

Next, from 107 µm to 277 µm (i.e., maximum peak value of the last peak corresponding to the increase in variance), for C1_LLDPE, the mean intensity starts to vary, with a decreasing tendency, to reach a lower intensity and then an intensity plateau at around 125. The variation of the mean intensity and the higher variance compared to the free

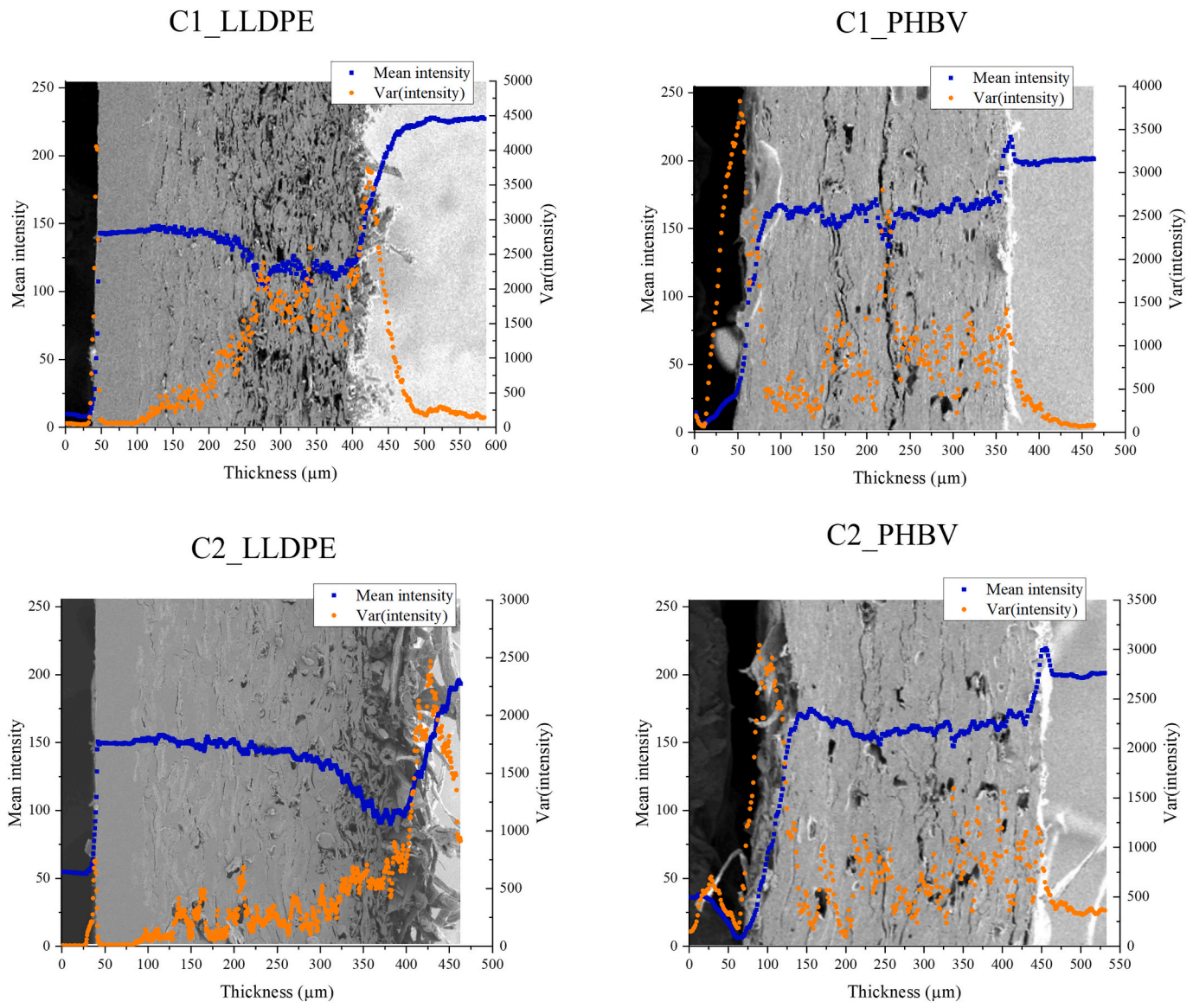

Fig. 5. Image analysis of SEM images for both C1- and C2-coated cardboards.

polymer layer are representative of the impregnated layer. In this layer, the polymer coexists with the cellulose matrix, with slightly different intensities, and where dark residual pores, with low intensity, increase the variance. In addition, the decreasing trend observed for the mean intensity combined with an increase in the variance can be explained by the presence of a gradient of impregnation. The closer to the free polymer layer, the more polymer will be impregnated, and this amount of polymer gradually decreases until it disappears, indicating the transition from the impregnated layer to the free cardboard layer. The impregnated layer and its boundaries can be difficult to identify depending on the structure of the material, as shown for C2_LLDPE where the final boundary of the layer is harder to distinguish. In this case, the same method was applied and the first maximum peak after the increase in variance was considered as the end of the impregnated layer. Finally, the range from 277 µm to 421 µm corresponds to the free cardboard layer, which is characterized by a low mean intensity, due to the porosity (dark areas), and high and increasing variance due to the structure of the cardboard and the proximity to the external atmosphere.

For both C1_PHBV and C2_PHBV, the mean intensity plot did not allow a thickness determination other than that of the total coated cardboard, as only a general slope was observed, with variations in both mean intensity and variance. This confirms the previous observations that only a single layer can be seen in the SEM images, namely the impregnated one, confirming a complete impregnation of the polymer. It is also worth noting that the image analysis of C1_PHBV highlights the structure of the commercial Cup Forma cardboard with a variance peak at 220 µm, which corresponds to the interphase between two layers of the uncoated cardboard.

Such image analyses were also performed on microtomography images but due to their low resolution, layers were harder to evidence as shown in the corresponding plots (Fig. 6). For C1_LLDPE, it is possible to evidence the free polymer layer as the part of the variance plot without significant variations (i.e., between 55 and 110). Apart from the free polymer layer, two different parts of the plot can be observed regarding the variance variation: first, decrease in variance until 275 µm, then steady values from 275 to 480 µm. Those two parts seem representative of the impregnated and the free cardboard layers respectively. It is worth noting that the impregnated layer seems to be inhomogeneous and might be a gradient of impregnation more than a strict layer. Thus, from the free coating layer until reaching the free cardboard layer, the proportion of polymer in the cardboard seem to decrease, leading to an increase in variance along the way. For C1_PHBV, analysis of X-ray

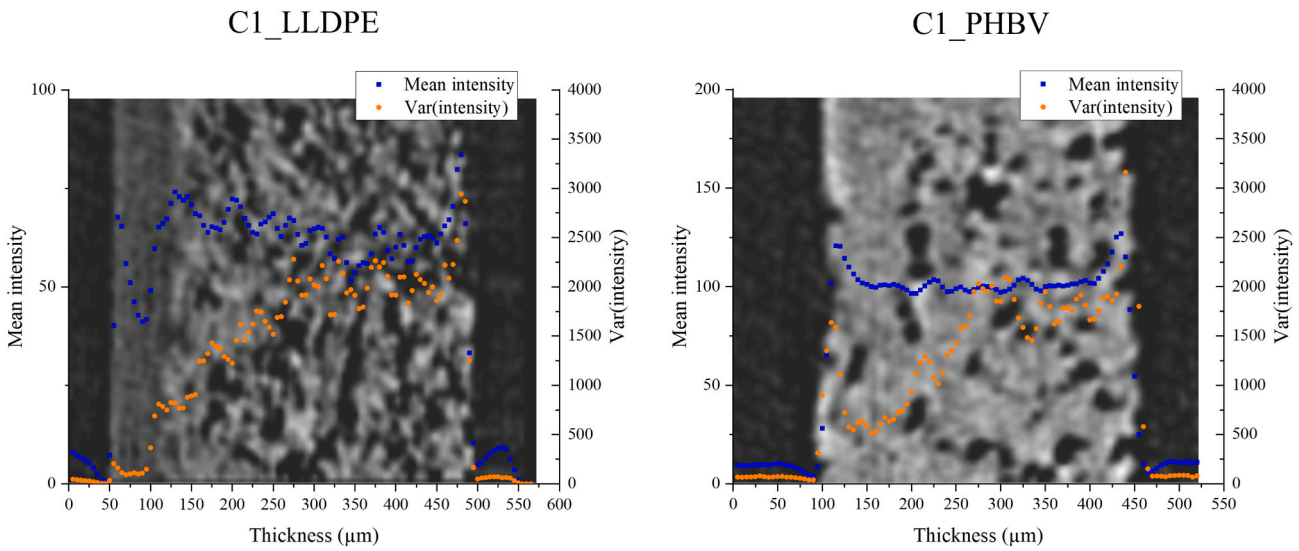

Fig. 6. Image analysis of microtomographs for (left) C1_LLDPE and (right) C1_PHBV.

microtomographs, and of the mean intensity, allows the identification of only one impregnated layer, which is congruent with SEM image analysis. When comparing to the C1_LLDPE microtomography, it is not possible to evidence any free cardboard layer in the case of C1_PHBV as the structure of the material is different from the structure of the cardboard layer. Thus, only an impregnated layer seems to be visible in the C1_PHBV microtomograph, with a gradient of impregnation and a stabilization.

Staining of the sample is usually performed to increase the density contrast of low-absorbing features in the sample [7,8,12,31,41,58]. Staining the cardboard before coating it with the polymer could have been tested to increase the contrast between the polymer and the cellulose fibers. However, it was hypothesized that this treatment could alter the surface properties of the constituents and therefore affect the impregnation mechanism of the polymer within the cardboard, but this was not investigated further in this study.

Even if it is possible to identify the layers on microtomographs, they are not as clear as in SEM images. Segmentation of µCT 2D images and 3D reconstruction have also been investigated using a machine learning-based approach. This is generally used for modeling approaches [32,33,36,37] or to investigate the interconnectivity of pores [32,34]. In the case of our coated cardboards, the resulting segmentation was very sensitive to the selected pixels. For a given microtomography, when one or the other pixel was selected for segmentation, the results were significantly different and did not allow a clear distinction between the three phases (i.e., polymer, fibers, and air) (Fig. S5). This can be attributed to both a low contrast difference between the phases and a low resolution of the images. This confirmed that SEM was preferable in general, even if both techniques can be used to determine all layer's thicknesses when the impregnation does not represent the entire coated cardboard thickness, i.e., when the impregnation remains partial.

Plotting the variance as well as the mean intensity allows for better detection of the layers. Indeed, when considering only the mean intensity, it is difficult to observe notable differences in the microtomographs, between the impregnated layer and the free cardboard layer whereas it is highlighted with the variance. Thus, analyzing images obtained from SEM and microtomography with this technique allows for the determination of the layers thickness. However, as shown in Supplementary materials, the presence of dust or defects on the cross-section of the coated cardboard affects the quality of the thickness determination (Fig. S4).

Thicknesses obtained from image analysis are listed in Table 2. For both C1 and C2 polymer-coated cardboards, structures obtained using

Table 2
Thickness values obtained from SEM and X-ray microtomography image analysis (mean values of profiles obtained on 1 and 4 SEM images for C1 and C2 coated cardboards respectively).

Materials	Imaging technique	Thicknesses (µm)		
		l_{fp}	l_i	l_{fc}
C1_PHBV	SEM	n.d.	308	n.d.
	Microtomography	n.d.	335	n.d.
C2_PHBV	SEM	n.d.	328 ± 19	n.d.
C1_LLDPE	SEM	65	170	144
	Microtomography	55	165	205
C2_LLDPE	SEM	64 ± 7	251 ± 28	47 ± 45

n.d.: not distinguishable.

PHBV and LLDPE are significantly different, which is congruent with SEM observations. Indeed, a total impregnation is obtained for PHBV coated cardboards whereas a partial impregnation is obtained using LLDPE, regardless of the cardboard used.

Regarding the impact of the cardboard's nature, since the global porosity values of C1 and C2 cardboard were close, i.e. 0.43 and 0.48 for C1 and C2 respectively, it was expected that resulting coated-cardboards structures would be similar. Three different observations were made for C2-coated cardboard as C2 represents the reference cardboard, i.e., without any multilayer structure, and one observation was made for both C1-coated cardboards as the intrinsic structures of C1 cardboards are more complex. Indeed, C1 cardboards are composed of an inner layer of sulphate pulp with chemi-thermomechanical pulp, between two layers of sulphate pulp [59]. This specific structure, highlighted by a variance peak at 220 for SEM image analysis of C1_PHBV, may decrease the impregnation of the polymer within the cardboard when the polymer reaches the middle layer. This can explain why, for C2_LLDPE, the impregnated layer thickness appears to be slightly higher than for C1_LLDPE.

3.2. Assessment of thicknesses based on the characterization of macroscopic physical parameters

3.2.1. Analytical model

Because the observation of the three layers can be challenging due to either the cutting step or the imaging technique resolution, and/or be time and cost-consuming, a mathematical model was developed to determine the three characteristic thicknesses (i.e. the thicknesses of the

free polymer layer, the impregnated layer, and the free cardboard layer) based on the characterization of macroscopic physical parameters (Fig. 7). Among them, the mass, and the surface of the uncoated, coated and control cardboards, noted m_{uc}, m_{cc}, m_c and S_{uc}, S_{cc}, S_c respectively, were measured and used as input parameters. It is worth noting that the surface of the uncoated cardboard is equal to the surface of the coated cardboard, as the coated cardboard is the result of the polymer coating on the uncoated cardboard. In addition, both the control and the coated cardboard thicknesses were assessed to determine the free polymer thickness. Finally, the value of both the polymer and the cellulose density are required.

This method should allow for the determination of the different thicknesses when advanced cutting and imaging techniques are not accessible. The main hypothesis of this analytical approach is that the polymer impregnates the cellulose substrate as a polymer front, that is the polymer fills all the pores as it penetrates the cardboard.

The first parameter to be calculated was the theoretical free polymer thickness (l_p). It represents the expected polymer thickness remaining on top of the cellulosic substrate if no impregnation occurs (Fig. 1a) and was calculated using Eq. (5):

$$l_p = \frac{cw}{d_{polymer}} \tag{5}$$

where cw is the coating weight (g.m^{-2}), and $d_{polymer}$ is the polymer density (g.m^{-3}).

If impregnation occurs, this leads to a reduced thickness of the free polymer layer (l_{fp}) as a part of the polymer penetrates the cardboard. If the thicknesses of the coated (l_c) and the control (l_{cc}) carboards could be measured on the same materials and at the same location, as is possible on a cross-sectional image, the free polymer layer could be expressed as follows (Eq. (6)):

$$l_{fp} = l_{cc} - l_c \tag{6}$$

Preliminary experimental results showed that the impregnation of the polymer into the cardboard mainly occurred after the full thermocompression of the cardboard (Fig. S6). This highlights that the porosity that should be used in the analytical model is the porosity of the thermocompressed cardboard, that is the control cardboard that underwent the same thermocompression cycle as the polymer-coated cardboard. The cardboard porosity (ϕ_c) can be expressed by Eq. (7):

$$\phi_c = \frac{V_{pores}}{V_c} \tag{7}$$

where V_{pores} is the volume of the pores in the cardboard (m^3) and V_c the total volume of the cardboard (m^3).

When all the pores of the impregnated layer are filled with the polymer, we can deduce that:

$$\phi_c = \frac{V_{p,i}}{V_i} = \frac{(l_p - l_{fp})}{l_i} \tag{8}$$

where $V_{p,i}$ is the volume of polymer that has impregnated (m^3) and V_i is the volume of the impregnated layer (m^3). The porosity accessible to the polymer, noted ϕ_a, can then be expressed as follows:

$$\phi_a = k^* \phi_c \tag{9}$$

where k corresponds to the proportion of the pores accessible to the polymer. Then, the thickness of the impregnated (l_i) was deduced from Eqs. (8) and (9):

$$l_i = k^* \frac{(l_p - l_{fp})}{\phi_a} \tag{10}$$

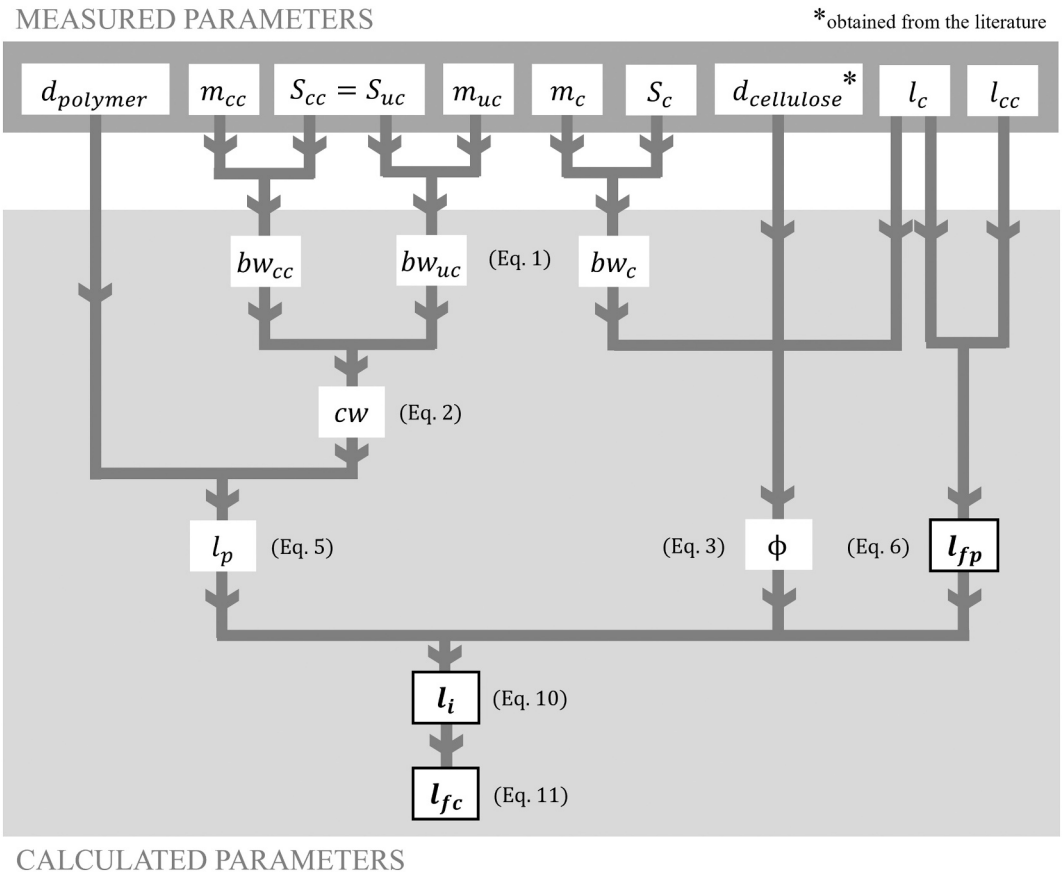

Fig. 7. Relationships between measured and calculated physical parameters.

Finally, the thickness of the free cardboard layer (l_{fc}) was deduced from the valued of the thickness of the free polymer layer and the thickness of the impregnated layer (Eq. (11)).

$$l_{fc} = l_{cc} - (l_{fp} + l_i) \quad (11)$$

However, the control cardboard and the coated cardboards are two distinct materials, which are necessarily characterized separately, leading to errors when applying Eq. (5). Indeed, as the values are not related to each other, such thickness subtraction can lead to negative values of the free polymer layer thickness. These negative values could also be caused by a high standard deviation in the measurement of coated cardboards and control cardboards total thicknesses. In our case, we want to estimate the final error on the thickness (which can be summarized as the general eq. C = A-B), accounting for the fact that (1) our measurements were performed independently of each other on different control and coated cardboards and that (2) it is physically impossible to have a negative C value (i.e., a negative thickness). In addition, to avoid making any extra and unnecessary assumptions about error distributions, a simple generic, distribution-free (in the sense that no parametric assumption is made about the errors) statistical estimator of the final error accounting for these aspects (independence and physical constraints) was developed. A corresponding statistical approach has been developed, an example of the approach is given in Supplementary material, and the MATLAB code is available in a dataset (doi:10.57745/D63VYY).

3.2.2. Validation of the analytical model

This developed analytical model was applied to the produced coated cardboards whose characteristics are listed in Table 3.

First, the results from the image analysis of the PHBV-coated cardboards were used to assess the actual accessible porosity of the C1 and C2 cardboards. These values of porosity accessible to the polymer can be determined using Eq. (8), using the analytical model and thickness values obtained using SEM image analysis. When applying these calculations, values of accessible porosity of 0.27 and 0.26 are obtained for C1 and C2 cardboards respectively.

When applying the analytical model to the produced coated cardboards, results show that regardless of the nature of the polymer, the impregnation seems to be only partial, that is the polymer does not fully penetrate the cardboard. However, the impregnation seems to be almost two times greater when coating PHBV on C1 cardboard than when coating LLDPE. This observation is not applicable to cardboard C2, where the impregnation of each polymer coating seems close. The obtained structure is illustrated in Fig. 8.

For PHBV-coated cardboards, while the image analysis results allow the observation of a fully impregnated cardboard, the analytical model indicates that the impregnation is partial. The thicknesses of impregnated layers were calculated and estimated to be 257 ± 39 µm and 270 ± 49 µm, whereas the SEM image analysis results in thicknesses of 308 and 328 ± 19 µm, for C1_PHBV and C2_PHBV, respectively, which, considering the standard deviation values, are close. For C1_PHBV, the impregnated layer thicknesses obtained from the analytical model and image analysis were close to one another and were not significantly different. However, it is important to highlight that no replicates of SEM were performed on C1-coated cardboard, as this cardboard was only used for comparison, and because of its complex intrinsic structure, it does not represent a model cardboard. A hypothesis for the observed difference in values between image analysis and the analytical model is that when the free polymer layer is thin, uncertainties regarding its thickness increase due to the resolution of the thickness measurement apparatus used, and this uncertainty will propagate into the analytical model. It is also worth noting that the surface homogeneity of the cardboard can vary from one point to another, thus making it more difficult to determine the coated cardboard and free polymer layer thicknesses.

For LLDPE-coated cardboards, the obtained thicknesses seem to be congruent with those obtained using image acquisition and analysis (Fig. 8c and d). Indeed, when considering the values of standard deviations, all three layers thicknesses were in the same data range, with a mean impregnated layer of approximately 167 ± 46 µm and 247 ± 45 µm for C1- and C2-coated cardboards respectively. A slight difference in the free polymer layer can be highlighted for C2_LLDPE, i.e. 88 ± 12 and 64 ± 7 for the analytical model and the image analysis respectively which may be explained by the determination of the coated cardboard thickness, which depends on the surface homogeneity of the cardboard.

3.2.3. Comparison of methods

The developed model presented various advantages compared with the other two methods tested. All tested methods have thus been ranked depending on multiple criteria, ranging from intrusiveness to accessibility (Table 4).

As previously discussed, microtomography does not allow clear visualization of the three characteristics layers leading to a lower precision while determining the layers thickness. This technique allows direct measurement without requiring sample preparation, whereas SEM, which requires a crucial cutting step, gives better precision in thickness determination due to the clear visualization of layers with adequate sample preparation. These techniques remain expensive and difficult to perform routinely.

Overall, the analytical model appears to be the simplest among the three investigated methods as thicknesses can be determined with a good precision despite moderate to high standard deviations while the technique remains accessible and simple of use. However, when using an analytical model, it is not possible to directly visualize the three layers.

A comparison of this developed analytical model to other methods from the literature allowing the quantitative assessment of the layers thicknesses is presented in Table 5.

Compared to experimental methods such as oil absorption, mercury absorption, and a calculation approach, the analytical method has various advantages. Besides the calculations used by Guillaume et al. [46], the oil and mercury absorption, as well as the analytical method, allowed the assessment of the impregnated layer thickness. However, the analytical model developed in this study is the only one that assesses the thickness of all the characteristic layers while remaining representative. Finally, it is worth noting that this method, as well as the calculation method, is non-destructive, which allows to further assess the properties of the samples.

4. Conclusion

To conclude, this article compares two methods for determining the thickness of the characteristic layers of a polymer-coated cardboard (i.e.,

Table 3
Denomination of materials and corresponding physical parameters (*cw* is the polymer coating weight in g·m^{-2}, bw_{cc} and bw_c are the basis weights of the polymer-coated cardboard and its associated control cardboard respectively, in g·m^{-2}, and l_{cc} and l_c are their respective thickness, in µm).

	Cardboard	Polymer	*cw* (g·m^{-2})	bw_c (g·m^{-2})	l_c (µm)	bw_{cc} (g·m^{-2})	l_{cc} (µm)
C1_PHBV	Cup Forma	PHBV	104.9 ± 0.1	264.67 ± 0.06	308 ± 17	373.30 ± 0.04	311 ± 8
C2_PHBV	B250	PHBV	121.3 ± 0.1	254.7 ± 0.2	327 ± 11	387.80 ± 0.09	354 ± 14
C1_LLDPE	Cup Forma	LLDPE	102.7 ± 0.1	265.7 ± 0.3	306 ± 11	371.30 ± 0.05	376 ± 7
C2_LLDPE	B250	LLDPE	124.8 ± 0.1	250.5 ± 0.4	316 ± 22	389.79 ± 0.06	376 ± 14

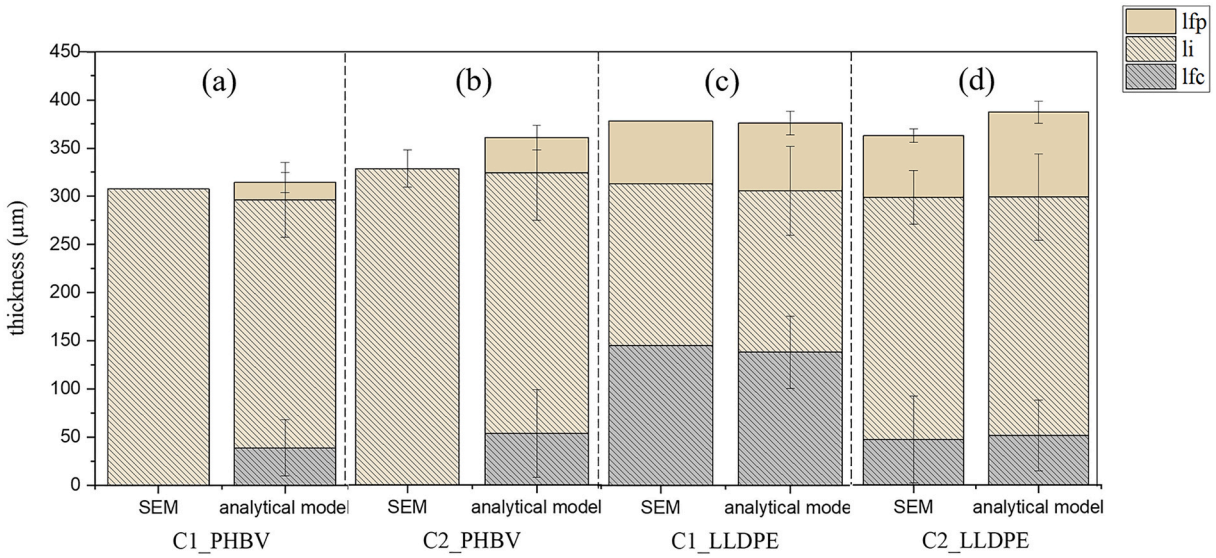

Fig. 8. Representation of the structure obtained using SEM image analysis (1 image for C1 coated cardboards and 4 for C2 coated carboards) and the analytical model for (a) C1_PHBV, (b) C2_PHBV, (c) C1_LLDPE and (d) C2_LLDPE. (Obtained values are collected in Table S6 in Supplementary materials).

Table 4
Comparison of the different methods for the determination of thicknesses.

Methods	Criteria						
	Direct measurement	Intrusiveness	Sample's preparation	Simplicity of use	Accessibility	Overall cost	Precision
Analysis of SEM images	Yes	=	Yes	=	+	++	++
Analysis of microtomography images	Yes	−	No	=	−	+	−
Analytical model	No	−−	No	++	++	−	+

Legends: −− very low, − low, = moderate, + high, ++ very high.

Table 5
Comparison of the analytical model to other methods from the literature.

Methods	Criteria					Source
	Free polymer layer	Impregnated layer	Free cardboard layer	Representativity	Destructive	
Analytical method	Thickness	Thickness	Thickness	++	No	n.a.
Oil absorption	No	Thickness	No	+	Yes	[47]
Mercury absorption	No	Thickness	No	+	Yes	[47]
Calculations	Thickness	Percentage	No	++	No	[46]

n.a. non applicable.

the free polymer layer, the impregnated layer, and the free cardboard layer). Both methods allowed the determination of all three thicknesses but differed in their accessibility and precision.

SEM in combination with image analysis, seems to be the methods allowing the best visualization of the three layers and to evidence a polymer impregnation gradient in the material. However, to obtain quantitative information using SEM, cutting the material to obtain a clean cross-section is still a crucial step as it can directly influence the image analysis. With microtomography, the sample does not need to be prepared, but the visualization of the three layers is not as clear as with SEM images, limiting its applicability due to the difficulty in determining thickness. The analytical model provides a more accessible way to determine the characteristic layers in polymer-coated cardboards. It is based on non-destructive measurements and can be used as a routine characterization. The results were congruent between the image analysis and the analytical model when replicates were performed. However, there is a need to further investigate the determination of the porosity accessible to the polymer in cardboards to obtain thicknesses that are representative of the coated cardboard, as the developed model it is highly dependent on this.

CRediT authorship contribution statement

Allison Vercasson: Writing – original draft, Visualization, Supervision, Software, Methodology, Investigation, Data curation, Conceptualization. **Sébastien Desterckе:** Writing – review & editing, Validation, Methodology, Formal analysis. **Nathalie Gontard:** Conceptualization. **Valérie Guillard:** Writing – review & editing, Validation, Supervision, Methodology, Funding acquisition, Conceptualization. **Hélène Angellier-Coussy:** Writing – review & editing, Validation, Supervision, Methodology, Funding acquisition, Conceptualization.

Declaration of competing interest

The authors declare that they have no known competing financial interests or personal relationships that could have appeared to influence the work reported in this paper.

Dataset

Data collected in the dataset corresponding to this study (doi:

10.57745/D63VYY) will be made available after acceptance of the present manuscript.

Acknowledgements

The authors acknowledge Aurélie Putois and Cécile Barron (IATE, Montpellier, France) for discussions and help on sample cutting techniques. The authors would also like to acknowledge Christine Lancelon-Pin and Joao Cosas Fernandes (CERMAV, Grenoble, France), for interesting discussion regarding sample preparation and cut. The authors also acknowledge Alexandre Léonard (Chemical Engineering, Liège University, Belgium) for the performing the mercury porosity measurements. Finally, the authors acknowledge Renaud Lebrun (ISEM, Montpellier, France) for the acquisition of the RX-microtomography and Véronique Viguier from the MEA platform (Université de Montpellier, France) for the SEM experiments and sample preparation.

Appendix A. Supplementary data

Supplementary data to this article can be found online at https://doi.org/10.1016/j.porgcoat.2024.108532.

References

[1] S. Sängerlaub, M. Brüggemann, N. Rodler, V. Jost, K.D. Bauer, Extrusion coating of paper with poly(3-hydroxybutyrate-co-3-hydroxyvalerate) (PHBV)-packaging related functional properties, Coatings 9 (2019), https://doi.org/10.3390/coatings9070457.
[2] N. Israni, S. Shivakumar, Polyhydroxyalkanoates in packaging, in: Biotechnological Applications of Polyhydroxyalkanoates, Springer Singapore, 2019, pp. 363–388, https://doi.org/10.1007/978-981-13-3759-8_14.
[3] E. Lo Faro, C. Menozzi, F. Licciardello, P. Fava, Improvement of paper resistance against moisture and oil by means coatings with poly(-3-hydroxybutyrate-co-3-hydroxyvalerate) (phbv) and polycaprolactone (pcl), Applied Sciences (Switzerland) 11 (2021), https://doi.org/10.3390/app11178058.
[4] C.G. Obeso, M.P. Sousa, W. Song, M.A. Rodriguez-Pérez, B. Bhushan, J.F. Mano, Modification of paper using polyhydroxybutyrate to obtain biomimetic superhydrophobic substrates, Colloids Surf. A Physicochem. Eng. Asp. 416 (2013) 51–55, https://doi.org/10.1016/j.colsurfa.2012.09.052.
[5] T. Cagnon, C. Guillaume, E. Gastaldi, N. Gontard, Importance of the structure of paper support in gas transfer properties of protein-coated paper, J. Appl. Polym. Sci. 130 (2013) 2848–2858, https://doi.org/10.1002/app.39509.
[6] M. Gällstedt, A. Brottman, M.S. Hedenqvist, Packaging-related properties of protein- and chitosan-coated paper, Packag. Technol. Sci. 18 (2005) 161–170, https://doi.org/10.1002/pts.685.
[7] G.C. Carrasco, T. Helle, Staining with OsO4 in the study of coated paper structure, Paperi Ja Puu 85 (2003). http://www.scioncorp.com.
[8] J. Lipponen, T. Lappalainen, Novel method for quantitative starch penetration analysis through iodine staining and image analysis of cross-sections of uncoated paper and board. https://www.researchgate.net/publication/279712432, 2005.
[9] S. Rivero, J. Lecot, A. Pinotti, Impregnation of kraft paper support with polylactic acid multilayers, Adv. Mater. Lett. 8 (2017) 741–751, https://doi.org/10.5185/AMLETT.2017.7107.
[10] P. Samyn, M. Deconinck, G. Schoukens, D. Stanssens, L. Vonck, H. Van Den Abbeele, Modifications of paper and paperboard surfaces with a nanostructured polymer coating, Prog. Org. Coat. 69 (2010) 442–454, https://doi.org/10.1016/J.PORGCOAT.2010.08.008.
[11] M. Shirazi, N. Esmail, G. Garnier, T.G.M. van de Ven, Starch penetration into paper in a size press, J. Dispers. Sci. Technol. 25 (2008) 457–468, https://doi.org/10.1081/DIS-200025714.
[12] R. Hagen, L. Salmén, Influence of the interaction zone between coating and paper on the dynamic mechanical properties of a coated paper, J. Mater. Sci. 30 (1995) 2821–2828, https://doi.org/10.1007/BF00349649.
[13] H. Aloui, K. Khwaldia, M. Ben Slama, M. Hamdi, Effect of glycerol and coating weight on functional properties of biopolymer-coated paper, Carbohydr. Polym. 86 (2011) 1063–1072, https://doi.org/10.1016/j.carbpol.2011.06.026.
[14] A. Mazega, Q. Tarrés, R. Aguado, M.À. Pèlach, P. Mutjé, P.J.T. Ferreira, M. Delgado-Aguilar, Improving the barrier properties of paper to moisture, air, and grease with nanocellulose-based coating suspensions, Nanomaterials 2022, Vol. 12, Page 3675 12 (2022) 3675. doi:https://doi.org/10.3390/NANO12203675.
[15] P. Nechita, The influence of coating composition on the structural and functional properties of coated paper for packaging applications, Nord Pulp Paper Res J 35 (2020) 408–418, https://doi.org/10.1515/npprj-2020-0029.
[16] K. Oh, K. Sim, Y. Bin Jung, H.J. Youn, H.L. Lee, Y.M. Lee, S.U. Yeu, Effect of coating binder on fold cracking of coated paper, Nord Pulp Paper Res J 30 (2015) 361–368, https://doi.org/10.3183/npprj-2015-30-02-p361-368.
[17] N. Sundar, Kumar S. Ananda, A. Pavithra, S. Ghosh, Studies on semi-crystalline poly lactic acid (PLA) as a hydrophobic coating material on kraft paper for imparting barrier properties in coated abrasive applications, Prog. Org. Coat. 145 (2020) 105682, https://doi.org/10.1016/J.PORGCOAT.2020.105682.
[18] H. Türe, M. Gällstedt, E. Johansson, M.S. Hedenqvist, Wheat-gluten/montmorillonite clay multilayer-coated paperboards with high barrier properties, Ind. Crop. Prod. 51 (2013) 1–6, https://doi.org/10.1016/j.indcrop.2013.08.054.
[19] A. Javed, H. Ullsten, L. Järnström, Effects on oxygen-barrier properties of pretreating paperboard with a starch-poly(vinyl alcohol) blend before polyethylene extrusion, Packag. Technol. Sci. 30 (2017) 399–410, https://doi.org/10.1002/pts.2210.
[20] E. Gastaldi, P. Chalier, A. Guillemin, N. Gontard, Microstructure of protein-coated paper as affected by physico-chemical properties of coating solutions, Colloids Surf. A Physicochem. Eng. Asp. 301 (2007) 301–310, https://doi.org/10.1016/j.colsurfa.2006.12.079.
[21] J. Kritzinger, W. Bauer, P. Salminen, J. Preston, A novel approach to quantify spatial coating-layer formation, TAPPI J. 9 (2010) 7–13, https://doi.org/10.32964/tj9.11.7.
[22] J. Kritzinger, U. Hirn, W. Bauer, Characterization of spatial coating layer formation - definition of a representative sample size, in: Advanced Coating Fundamentals Symposium, Montreal, 2008. https://www.researchgate.net/publication/267694082.
[23] M. Wiltsche, M. Donoser, J. Kritzinger, W. Bauer, Automated serial sectioning applied to 3D paper structure analysis, J. Microsc. 242 (2011) 197–205, https://doi.org/10.1111/j.1365-2818.2010.03459.x.
[24] M. Myllys, H. Häkkänen, J. Korppi-Tommola, K. Backfolk, P. Sirviö, J. Timonen, X-ray microtomography and laser ablation in the analysis of ink distribution in coated paper, J. Appl. Phys. 117 (2015), https://doi.org/10.1063/1.4916588.
[25] B. Ghanbarian, H. Aslannejad, A. Raoof, Modeling water imbibition into coated and uncoated papers, Chem. Eng. Sci. 189 (2018) 33–42, https://doi.org/10.1016/j.ces.2018.05.051.
[26] H. Aslannejad, S.M. Hassanizadeh, M.A. Celia, Characterization of the interface between coating and fibrous layers of paper, Transp. Porous Media 127 (2019) 143–155, https://doi.org/10.1007/s11242-018-1183-2.
[27] H. Aslannejad, S.M. Hassanizadeh, A. Raoof, D.A.M. de Winter, N. Tomozeiu, M. T. van Genuchten, Characterizing the hydraulic properties of paper coating layer using FIB-SEM tomography and 3D pore-scale modeling, Chem. Eng. Sci. 160 (2017) 275–280, https://doi.org/10.1016/j.ces.2016.11.021.
[28] J. Viguié, P. Latil, L. Orgéas, P.J.J. Dumont, S. Rolland du Roscoat, J.F. Bloch, C. Marulier, O. Guiraud, Finding fibres and their contacts within 3D images of disordered fibrous media, Compos. Sci. Technol. 89 (2013) 202–210, https://doi.org/10.1016/j.compscitech.2013.09.023.
[29] C. Marulier, P.J.J. Dumont, L. Orgéas, S. Rolland du Roscoat, D. Caillerie, 3D analysis of paper microstructures at the scale of fibres and bonds, Cellulose 22 (2015) 1517–1539, https://doi.org/10.1007/s10570-015-0610-6.
[30] T. Walther, H. Thoemen, K. Terzic, H. Meine, New opportunities for the microstructural analysis of wood fibre networks. http://kogs-www.informatik.uni, 2006.
[31] J.M. Silva, I. Zanette, P.B. Noël, M.B. Cardoso, M.A. Kimm, F. Pfeiffer, Three-dimensional non-destructive soft-tissue visualization with X-ray staining micro-tomography, Sci. Rep. 5 (2015) 1–7, https://doi.org/10.1038/srep14088.
[32] D.S. Carrillo, F. Jian, D.S. Jayas, J. Paliwal, Characterisation of pore structure of bulk wheat mixed with dockage using X-ray micro-computed tomography and deep learning, Biosyst. Eng. 240 (2024) 62–76, https://doi.org/10.1016/j.biosystemseng.2024.03.001.
[33] K. Liu, Y. Wang, Pore structure characterization and effective thermal conductivity modeling of fibrous building thermal insulation materials based on X-ray tomography, International Communications in Heat and Mass Transfer 154 (2024), https://doi.org/10.1016/j.icheatmasstransfer.2024.107410.
[34] T. Ilzig, D. Schumacher, M. Wilhelm, S. Günther, S. Odenbach, Image data analysis of high resolution µCT data for the characterization of pore orientation and pore space interconnectivity in freeze cast ceramics, Mater. Charact. 174 (2021), https://doi.org/10.1016/j.matchar.2021.110966.
[35] M. Wu, H. Li, L. Wang, X. Yang, C. Dai, N. Yang, J. Li, Y. Wang, M. Yu, µCT quantitative assessment of the pore–fracture structures and permeability behaviors of long-flame coal treated by infrared rapid heating, Energy 274 (2023) 127308, https://doi.org/10.1016/J.ENERGY.2023.127308.
[36] J.A. Hannun, R.I. Al-Raoush, Z.A. Jarrar, K.A. Alshibli, J. Jung, Fines effect on gas flow in sandy sediments using µCT and pore networks, J. Nat. Gas Sci. Eng. 108 (2022) 104834, https://doi.org/10.1016/J.JNGSE.2022.104834.
[37] Z. Zhao, X.P. Zhou, Pore-scale diffusivity and permeability evaluations in porous geomaterials using multi-types pore-structure analysis and X-µCT imaging, J Hydrol (Amst) 615 (2022) 128704, https://doi.org/10.1016/J.JHYDROL.2022.128704.
[38] W. Hübner, Studying the pore space of cuttings by NMR and µCT, J. Appl. Geophys. 104 (2014) 97–105, https://doi.org/10.1016/J.JAPPGEO.2014.02.016.
[39] C.L. Reedy, C.L. Reedy, High-resolution micro-CT with 3D image analysis for porosity characterization of historic bricks, Herit. Sci. 10 (2022), https://doi.org/10.1186/S40494-022-00723-4.
[40] G. Pyka, G. Kerckhofs, J. Schrooten, M. Wevers, The effect of spatial micro-CT image resolution and surface complexity on the morphological 3D analysis of open porous structures, Mater. Charact. 87 (2014) 104–115, https://doi.org/10.1016/J.MATCHAR.2013.11.004.
[41] J.L. Paris, F.A. Kamke, Quantitative wood–adhesive penetration with X-ray computed tomography, Int. J. Adhes. Adhes. 61 (2015) 71–80, https://doi.org/10.1016/J.IJADHADH.2015.05.006.
[42] A. Cherpinski, S. Torres-Giner, J. Vartiainen, M.S. Peresin, P. Lahtinen, J. M. Lagaron, Improving the water resistance of nanocellulose-based films with

polyhydroxyalkanoates processed by the electrospinning coating technique, Cellulose 25 (2018) 1291–1307, https://doi.org/10.1007/s10570-018-1648-z.
[43] A. Adibi, D. Valdesueiro, L. Simon, C.P. Lenges, T.H. Mekonnen, High barrier sustainable paper coating based on engineered polysaccharides and natural rubber, ACS Sustain. Chem. Eng. 10 (2022) 10718–10732, https://doi.org/10.1021/ACSSUSCHEMENG.2C03466/ASSET/IMAGES/LARGE/SC2C03466_0011.JPEG.
[44] J. Cosas, V.H. Mareau, L. Gonon, AFM-Raman colocalization setup: advanced characterization technique for polymers, Int. J. Polym. Anal. Charact. 23 (2017) 113–119, https://doi.org/10.1080/1023666X.2017.1391740.
[45] H. Kjellgren, G. Engström, Influence of paper structure on barrier properties of starch-coated greaseproof paper, Nord Pulp Paper Res J 23 (2008) 87–90.
[46] C. Guillaume, J. Pinte, N. Gontard, E. Gastaldi, Wheat gluten-coated papers for bio-based food packaging: structure, surface and transfer properties, Food Res. Int. 43 (2010) 1395–1401, https://doi.org/10.1016/j.foodres.2010.04.014.
[47] M. Khlewee, W. Desisto, D. Bousfield, Comparison of methods to characterize the penetration of hot melt adhesive into paper, Nord Pulp Paper Res J (2022), https://doi.org/10.1515/npprj-2022-0066.
[48] M. Khlewee, W.J. DeSisto, D.W. Bousfield, Prediction of non-isothermal polymer penetration into porous layers, Ind. Eng. Chem. Res. (2023), https://doi.org/10.1021/acs.iecr.3c00782.
[49] F. Biddlestone, A. Harris, J.N. Hay, T. Hammond, The physical ageing of amorphous poly(hydroxybutyrate), Polymer (Guildf) 39 (1996) 221–229, https://doi.org/10.1002/(SICI)1097-0126(199603)39:3.
[50] J. Schindelin, I. Arganda-Carreras, E. Frise, V. Kaynig, M. Longair, T. Pietzsch, S. Preibisch, C. Rueden, S. Saalfeld, B. Schmid, J.Y. Tinevez, D.J. White, V. Hartenstein, K. Eliceiri, P. Tomancak, A. Cardona, Fiji: an open-source platform for biological-image analysis, Nat. Methods 9 (2012) 676–682, https://doi.org/10.1038/nmeth.2019.
[51] M. Antlauf, N. Boulanger, L. Berglund, K. Oksman, O. Andersson, Thermal conductivity of cellulose fibers in different size scales and densities, Biomacromolecules 22 (2021) 3800–3809, https://doi.org/10.1021/ACS.BIOMAC.1C00643.
[52] J.H. Han, J.M. Krochta, Physical properties and oil absorption of whey-protein-coated paper, J. Food Sci. 66 (2001) 294–299, https://doi.org/10.1111/j.1365-2621.2001.tb11335.x.
[53] B.N. Altay, A. Huq, B. Aksoy, R. Hailstone, M. Demir, C. Aydemir, A. Karademir, S. Williams, Enhanced internal coating structure and light reflectance of coated papers: a sludge valorization process, ACS Sustain. Chem. Eng. (2023), https://doi.org/10.1021/ACSSUSCHEMENG.3C00566/ASSET/IMAGES/LARGE/SC3C00566_0013.JPEG.
[54] P. Nuchanong, M. Seadan, R. Khankrua, S. Suttiruengwong, Thermal stability enhancement of poly(hydroxybutyrate-co-hydroxyvalerate) through in situ reaction, Des. Monomers Polym. 24 (2021) 113–122, https://doi.org/10.1080/15685551.2021.1914406.
[55] B. Sun, L. Dang, Q. Bi, R. Li, Q. Gong, Z. Wan, S. Xu, Effect of different compatibilizers on the mechanical, flame retardant, and rheological properties of highly filled linear low-density polyethylene/magnesium hydroxide composites, Polymers (Basel) 15 (2023) 4115, https://doi.org/10.3390/polym15204115.
[56] J. Ghassemzadeh, M. Hashemi, L. Sartor, M. Sahimi, Pore network simulation of imbibition into paper during coating: I, Model development, AIChE Journal 47 (2001) 519–535, https://doi.org/10.1002/AIC.690470303.
[57] A. Le Duigou, A. Kervoelen, A. Le Grand, M. Nardin, C. Baley, Interfacial properties of flax fibre-epoxy resin systems: existence of a complex interphase, Compos. Sci. Technol. 100 (2014) 152–157, https://doi.org/10.1016/j.compscitech.2014.06.009.
[58] E. Purington, A.R. Blakeley, D. Bousfield, W.M. Gramlich, Visualization of latex and starch in paper coatings by tagging with fluorescent dyes, Nord Pulp Paper Res J 32 (2017) 395–406, https://doi.org/10.3183/npprj-2017-32-03-p395-406.
[59] Stora Enso, Technical specification - Cupforma Nature. https://www.storaenso.com/en/products/paperboard-materials/foodservice-packaging. (Accessed 26 July 2023) (n.d.).